Supplementary Information

Selective production of acetonitrile by dehydroamination of ethanol over a stable Cu-Zr/meso SiO_2 catalyst

Xiaomin Zhang[a,b], Mo Zhou[b], Yujia Zhao[b], Jifeng Pang[b], Pengfei Wu[b,*], Zhen Guo[c,d,*] and Mingyuan Zheng[b,*]

[a] School of Transportation Engineering, Dalian Jiaotong University, Dalian 116028, China

[b] CAS Key Laboratory of Science and Technology on Applied Catalysis, Dalian Institute of Chemical Physics, Chinese Academy of Sciences, Dalian 116023, China

[c] School of Materials Science and Engineering, Dalian Jiaotong University, Dalian 116028, China

[d] Key Laboratory of Agricultural Resource Chemistry and Biotechnology, Yulin 537000, China

Chemical reagents

$ZrO(NO_3)_2$ (99.5 wt%) , urea (99 wt%), Al_2O_3 (99.9 wt%), TiO_2 (99.8 wt%), ZrO_2 (99 wt%), silica sol (40 wt%), nano SiO_2 (99.5 wt%), ammonium carbonate (99 wt%), tetraethyl orthosilicate (TEOS, 98 wt%), nitric acid (65-68 wt%), 1-butanol (99 wt%), 1-pentanol (99 wt%), 1-hexanol (99 wt%), 1-heptanol (98 wt%), 1-octanol (99 wt%), isobutanol (99 wt%), benzyl alcohol (99 wt%), acetonitrile (99 wt%), butyronitrile (99 wt%), pentanonitrile (97 wt%), hexanenitrile (97 wt%), heptanonitrile (98 wt%), octanenitrile (97 wt%), isobutylronitrile (99 wt%), benzonitrile (99 wt%), 2-methylpyridine (98 wt%), 4-methylpyridine (98 wt%), diethylamine (99.5 wt%) and triethylamine (99.5 wt%) were purchased from Shanghai Aladdin Biochemical Technology Co., Ltd. $Cu(NO_3)_2{\cdot}3H_2O$ (99 wt%) and ethanol (99.7 wt%) were purchased from Sinopharm Chemical Reagent Co, Ltd. MFI was purchased from Tianjin Nanhua Catalyst Co., Ltd. $Mn(NO_3)_2{\cdot}6H_2O$ (98 wt%), $Cr(NO_3)_2{\cdot}9H_2O$ (99 wt%), $Fe(NO_3)_2{\cdot}9H_2O$ (98.5 wt%), $Ni(NO_3)_2{\cdot}6H_2O$ (98 wt%), $Ce(NO_3)_3{\cdot}6H_2O$ (99.5 wt%), $Ga(NO_3)_2$ (99.9 wt%), $In(NO_3)_3$ (99.9 wt%), $La(NO_3)_3{\cdot}6H_2O$ (99 wt%), $LiNO_3$ (99 wt%), $Co(NO_3)_2{\cdot}6H_2O$ (98.5 wt%), $Gd(NO_3)_2{\cdot}4H_2O$ (99 wt%) and $Sc(NO_3)_3{\cdot}6H_2O$ (99 wt%) were purchased from Shanghai Macklin Biochemical Co., Ltd. Meso SiO_2 (99.5 wt%, $S_{BET} \geq 400\ m^2/g$) was purchased from Qingdao Haiwan Specialty Chemicals Co., Ltd.

Characterization

Powder X-ray diffraction (XRD) patterns were recorded on a PANalytical X'Pert-Pro X-ray diffractometer with a Cu Kα radiation (λ = 0.154059 nm) operating at 40 kV and 40 mA. The chemical composition of the samples was determined using a Philips Magix-601 X-ray fluorescence (XRF) spectrometer. The metal loading of spent catalysts was determined by inductively coupled plasma optical emission spectroscopy (ICP-OES) on a Thermo iCAP6300 instrument. Before analysis, the catalyst was dissolved in aqua regia (3 mL HCl and 1 mL HNO3), and then diluted into 1-10 ppm according to the theoretical amount of metals. High-angle annular dark field scanning transmission electron microscopy (HAADF-STEM) images and energy dispersive X-ray spectra (EDX) elemental mapping of samples were obtained by using a JEOL JEM-2100F microscope, operated at 200 kV. Temperature-programmed reduction (H_2-TPR) was carried out on a Micromeritics AutoChem II 2920 instrument equipped with a thermal conductivity detector (TCD). About 100 mg of calcined catalyst was loaded into a quartz tube and dried in argon stream at 150 °C for 1 h to remove the adsorbed water. After being returned to 50 °C, the catalyst was heated in a 10 % H_2-Ar flow at a heating rate of 10 °C/min up to 500 °C. The copper dispersion and the surface area of metallic copper of catalysts were determined by the N_2O chemisorption method. The catalyst was first reduced in the procedure described in the TPR experiment in 10% H_2/Ar until 350 °C. The amount of hydrogen consumption in the first TPR was denoted as A_1. Then, the reactor was purged with Ar at 50 °C and a flow of 10% N_2O/Ar was used to oxidize surface copper atoms to Cu_2O at 50 °C for 1 h. After flushing with Ar to remove the oxidant, another TPR experiment was performed in 10% H_2/Ar until 350 °C. Hydrogen consumption in the second TPR was denoted as A_2. The dispersion (D_{Cu}) of surface Cu were calculated by the following equation (Equation 1):

$$D_{Cu} = \frac{2A_2}{A_1} \times 100\% \quad \text{(Equation 1)}$$

Specific area of metallic copper (S_{Cu}) and Cu particle size (d_{Cu}) were calculated according to following equations (Equations 2-3):[1, 2]

$$S_{Cu} = \frac{2A_2 \times N_{av}}{A_1 \times M_{Cu} \times 1.46 \times 10^{19}} \ (m^2{}_{Cu}/g_{Cu}) \quad \text{(Equation 2)}$$

$$d_{Cu} = \frac{6000}{S_{Cu} \times \rho_{Cu}} \ (nm) \quad \text{(Equation 3)}$$

ρ_{Cu} is the density of copper (8.92 g/cm^3), N_{av} is Avogadro's constant (6.02 × 10^{23}/mol), M_{Cu} is the relative atomic mass of copper (63.46 g/mol), and 1.46 × 10^{19} is the number of copper atom of per square meter.

Ex-situ X-ray photoelectron spectra (XPS) were recorded on a Thermo Scientific K-Alpha+ spectrometer with a monochromatic Al-Kα X-ray source as the excitation source. Prior to the test, the calcined sample was firstly compressed into a thin disk and reduced in a 10 % H_2-Ar flow of 50 mL/min at 300 °C for 4 h and cooled naturally. Then, the pre-reduced sample was passivated in a 1 % O_2-Ar flow of 20 mL/min for 8 h. Afterwards, the sample was carefully transferred into the XPS measurement chamber under high vacuum condition (P < 10^{-9} Pa). Energy corrections were performed using a 1s peak of the polluted carbon at 284.6 eV. Nitrogen adsorption isotherms were measured at -196 °C on a Micromeritics ASAP 2460 system. Before the measurements, all samples were pretreated in vacuum at 300 °C for 8 h. The total surface area was calculated based on the Brunauer–Emmett–Teller (BET) equation. The micropore volume was evaluated using the *t*-plot method. The mesopore volume was evaluated from the adsorption isotherm by the Barrett–Joyner–Halenda (BJH) method. NH_3 temperature-programmed desorption (NH_3-TPD) was performed on Micromeritics Autochem II apparatus equipped with a mass spectrometer (MS) detector. Typically, 100 mg of sample was pretreated at 300 °C for 60 min in He flow of 30 mL/min. After cooling down to 50 °C, NH_3 was dosed onto the sample until its saturated adsorption. Then the sample was purged with He flow for 30 min to remove the physically absorbed NH_3. Finally, the sample was heated to 800 °C at a rate of 10 °C/min, and the NH_3 desorbed from the surface and was monitored by the MS detector. Fourier transform infrared (FTIR) spectra were collected on a Bruker Tensor 27 instrument. For the adsorption measurements, 20 mg catalyst was pressed into a self-supporting disc and mounted on the sample holder. The catalysts were activated under vacuum (p = 10^{-6} mbar) at 350 °C for 1 h. As soon as the catalyst cooled to 150 °C, a spectrum of the activated catalyst was taken as the background. Subsequently, adsorption of pyridine was performed at 0.1 mbar for 30 min until saturation/equilibration of the surface was reached and the peak area of the IR signal remained

constant. After physisorbed pyridine was removed by evacuation (p = 10^{-6} mbar) at 150 °C, another spectrum was recorded. Finally, spectra were taken after desorption at 150 °C, 250 °C, and 350 °C for 30 min, respectively, and then the FTIR spectra were collected at ambient temperature. The acid sites quantity was calculated by following equations (Equations 4-5):[3]

$$C_{\text{pyridine on Brönsted sites}} = \frac{1.88 \times \text{IA(B)} \times R^2}{W} \quad \text{(Equation 4)}$$

$$C_{\text{pyridine on Lewis sites}} = \frac{1.42 \times \text{IA(L)} \times R^2}{W} \quad \text{(Equation 5)}$$

C is the acid sites density (mmol/g), IA (B or L) is the integrated absorbance of B or L bands (cm^{-1}), R is the radius of catalyst sample disk (cm), W is the weight of catalyst sample disk (mg).

The adsorption and desorption isotherms of ethanol and acetonitrile were determined using an Intelligent Gravimetric Analyzer (IGA). About 25 mg sample was added to the chamber and outgassed until reaching to a constant weight at 250 °C. Then the flowrate of ethanol or acetonitrile vapor was introduced. The adsorption kinetics curve was recorded at a pressure of 5 mbar, 40 °C. The desorption kinetics curve was recorded from a pressure of 2 mbar, 40 °C. Thermogravimetric analysis (TG) was performed on a TA SDTQ600 analyzer. Measurements were performed in the temperature range of 25-800 °C with a temperature-programmed rate of 10 °C/min in continuous flow of synthetic air (100 mL/min).

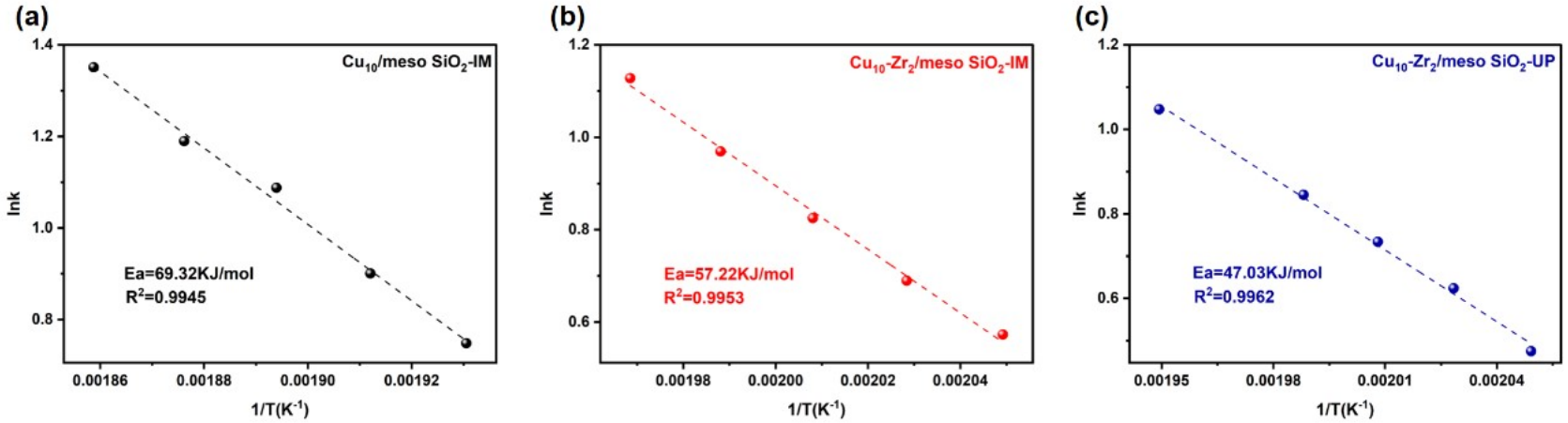

Figure S1. Arrhenius plots for the conversion of ethanol over catalysts. Reaction conditions: p = 0.1 MPa, ethanol WHSV = 7 h^{-1}, NH_3/ethanol molar ratio = 3.

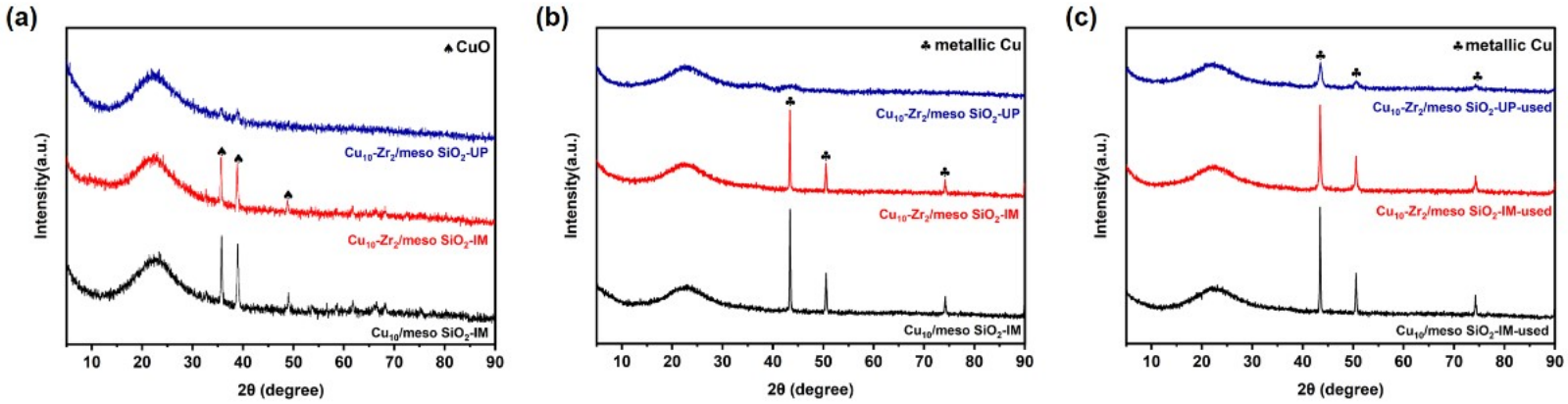

Figure S2. XRD patterns of the (a) calcined (b) reduced and (c) spent catalysts.

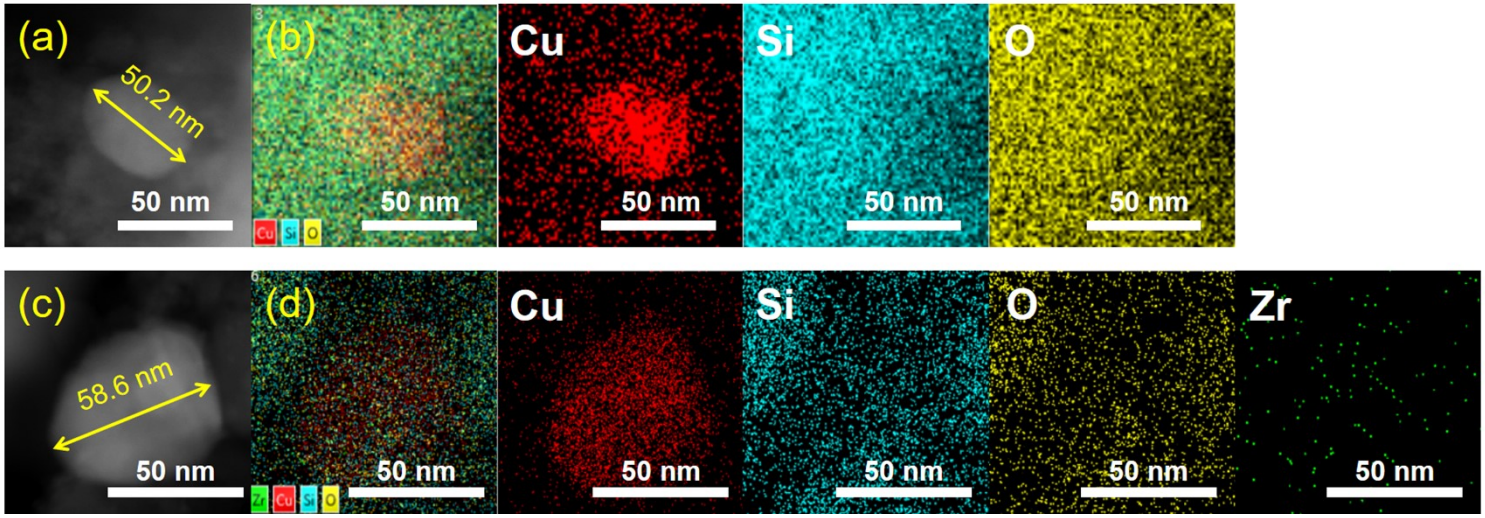

Figure S3. HAADF-STEM images and corresponding elemental mappings of Cu_{10}/meso SiO_2-IM (a,b) and Cu_{10}-Zr_2/meso SiO_2-IM (c,d).

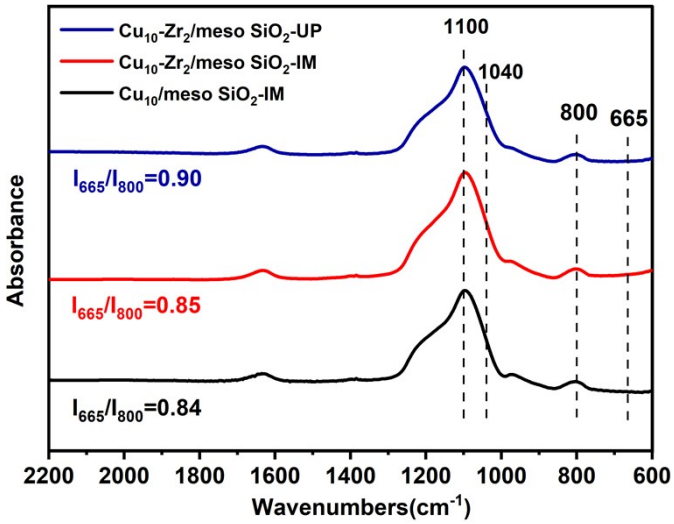

Figure S4. FTIR spectra of the as-calcined catalysts. The I_{665}/I_{800} intensity ratio represents the relative amount of copper phyllosilicate in the samples.

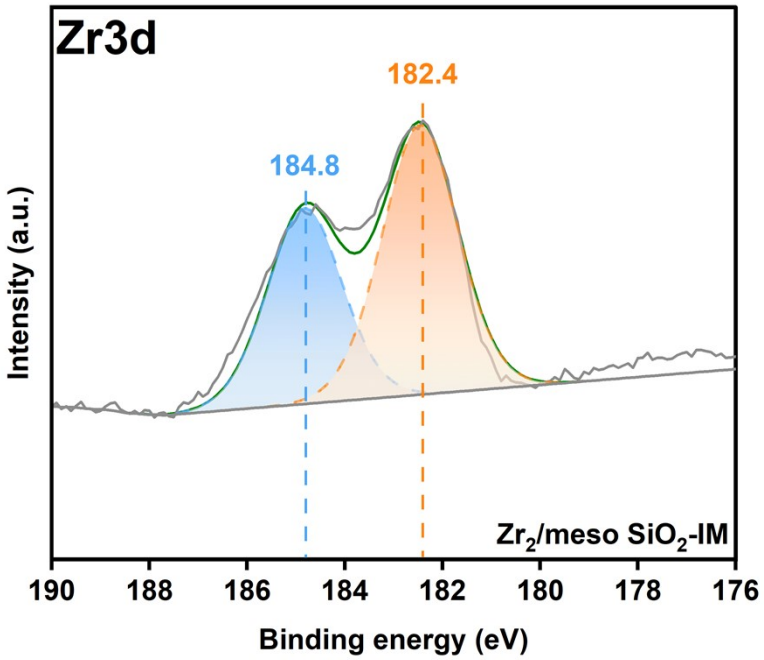

Figure S5. Zr 3d XPS spectrum of reduced Zr_2/meso SiO_2-IM.

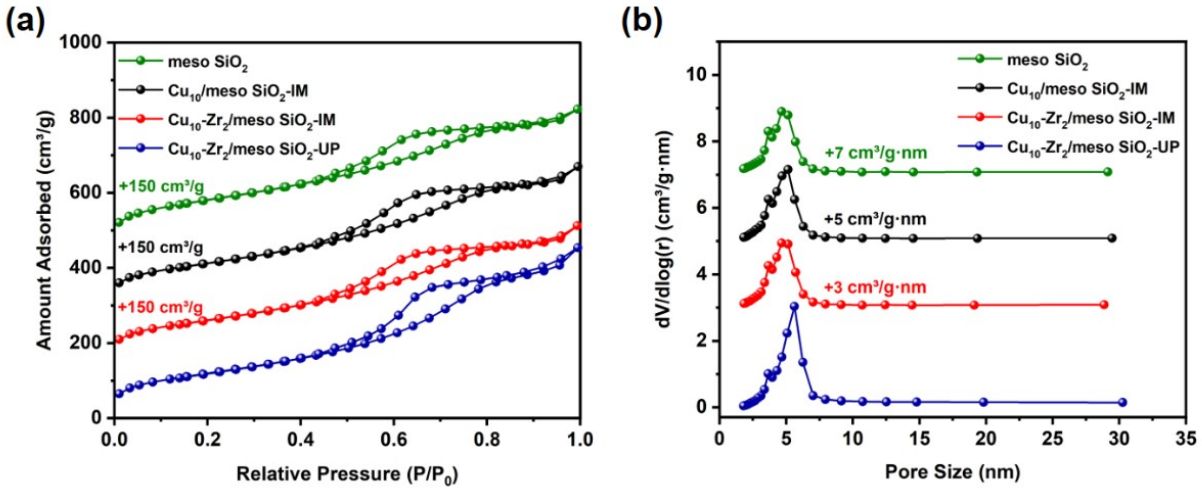

Figure S6. (a) N_2 adsorption-desorption isotherms and (b) pore size distribution of samples.

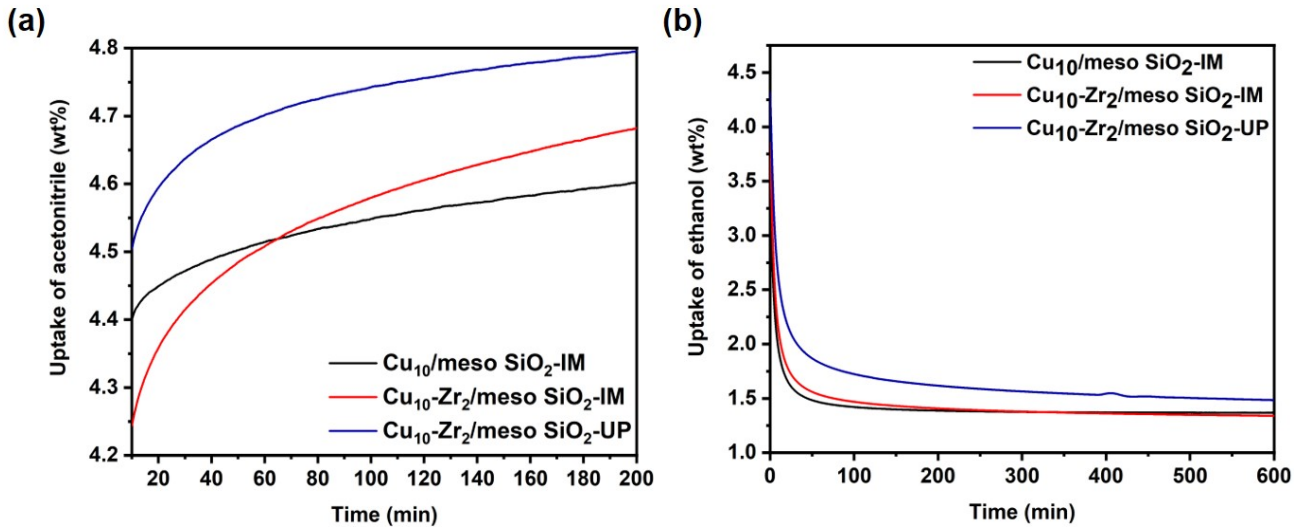

Figure S7. IGA curves of acetonitrile adsorption (a) and ethanol desorption (b) over catalysts.

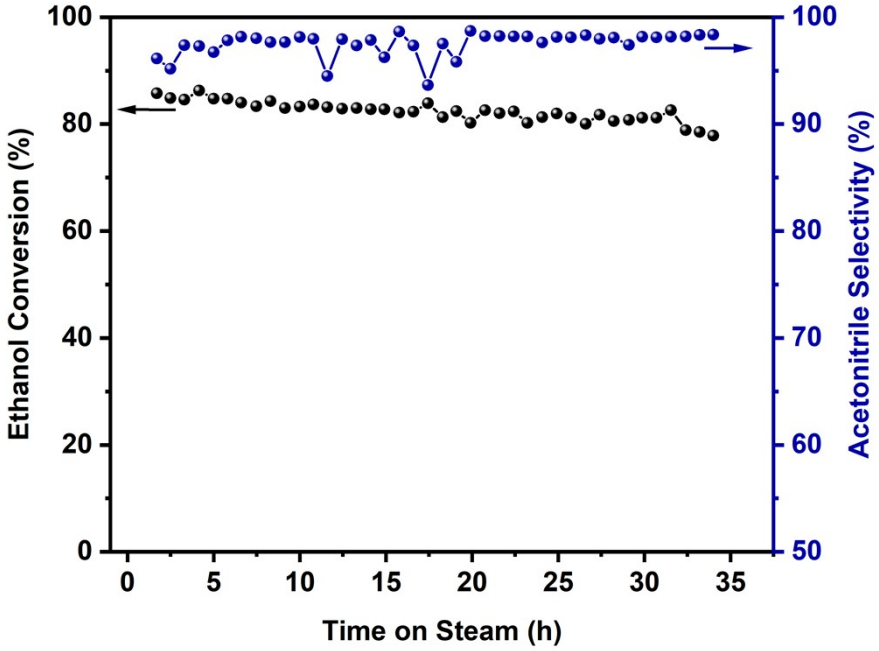

Figure S8. Ethanol conversion and acetonitrile selectivity variation with time-on-stream over regenerated Cu_{10}-Zr_2/meso-SiO_2-UP. (Reaction conditions: p = 0.1 MPa, T = 265 °C, ethanol WHSV = 0.8 h^{-1}, NH3/ethanol molar ratio = 9.)

Table S1. Performance and characteristics of the synthetic routes for acetonitrile production

Synthetic routes		Feedstock	Reaction temperature	Conversion (%)	Selectivity (%) or productivity	Characteristics	AE [a]	E-factor [b]	Ref.
Commercial propylene ammoxidation (SOHIO) process		Propylene, NH_3, O_2	470-480 °C	95	2-4, as by-product	Complex and toxic by-products (HCN, propionitrile, acrolein, acetone, acetaldehyde, allyl alcohol, oxazole, benzonitrile, etc.); energy-intensive separation process; productivity constraint	38.3%	25.02	4
C1 substrates	Carbon monoxide hydroamination	Carbon monoxide, NH_3, H_2	475 °C	47	96	Poor activity, unmentioned catalyst stability	53.3%	0.99	5
	Methane amination	Methane, NH_3	700 °C	3.5	372.4 $\mu mol/g_{Ga}/min$	High reaction temperature, inferior catalyst stability, toxic by-product of HCN, co-production of H_2	83.7%	1.91	6
	Methanol amination	Methanol, NH_3	525 °C	98	63	Insufficient catalytic lifetime (<60 hours), renewable catalyst, toxic by-product of HCN, co-production of H_2	50.6%	2.14	7
C2 substrates	Ethylene dehydroamination	Ethylene, NH_3	500 °C	20	80	Poor activity, inferior catalyst stability, toxic by-product of HCN, co-production of H_2	91.1%	1.04	8
	Ethylene ammoxidation	Ethylene, NH_3, O_2	500 °C	15-26	95-97	Poor activity, unmentioned catalyst stability	44.1%	1.72	9, 10
	Ethane dehydroamination	Ethane, NH_3	500 °C	15-20	20-68	Poor activity, inferior catalyst stability, toxic by-product of HCN, co-production of H_2	87.2%	1.02	8, 11
	Ethane ammoxidation	Ethane, NH_3, O_2	400-450 °C	10-48	25-90	Poor reactivity, unmentioned catalyst stability	43.1%	1.71	12-19

Acetic acid amination	Acetic acid, NH_3	360-390 °C	88-99	62-99	High activity, high corrosiveness on equipment, inferior catalyst stability	53.3%	0.96	[20]
Ethylamine aerobic dehydrogenation	Ethylamine, O_2	225 °C	99	80	Costly feedstock, inferior catalyst stability	44.1%	1.45	[21]
Ethylamine electrocatalytic dehydrogenation	Ethylamine	Room temperature	-	55-99	Costly feedstock, high Faraday efficiency, low production capacity, inferior cycling stability	91.1%	-	[22-25]
Ethanol ammoxidation	Ethanol, NH_3, O_2	350-450 °C	80-99	45-95	High activity, renewable substrate, inferior catalyst stability	36.9%	1.46	[26-31]
Ethanol dehydroamination	Ethanol, NH_3	230-450 °C	91-99/(96, this work)	69-98/(96, this work)	High activity, renewable substrate, co-production of H_2, insufficient catalytic lifetime (<hundreds of hours)	65.1%	0.57/(0.60, this work)	[32-45]

[a] Atom economy, defined as the molecular weight ratio of the target product to the sum of all reactants. [b] Environmental factor, defined as mass ratio of total waste to target product. Calculation based on optimal reaction performance.

Table S2. Results of catalytic dehydroamination of ethanol over copper-based catalysts

Catalyst	Reaction Condition	Acetonitrile yield (%)	Ref.
Cu_{10}-Zr_2/meso SiO_2-UP	265 °C, 0.1 MPa, n(NH_3):n(alcohol)=9:1, LHSV=0.8 h^{-1}	95	This work
15%Cu/Al_2O_3	325 °C, 0.1 MPa, Cu/Al_2O_3 (3 mL), $V_{(alcohol)}$=0.1 mmol/min, n(NH_3):n(alcohol)=20:1	87	[32]
Cu/γ-Al_2O_3	290 °C, 0.1 MPa, n(NH_3):n(alcohol)=7:1, WHSV=1.0 h^{-1}	92	[33]
15%Cu/Na-ZSM-23	350 °C, 0.1 MPa, n(NH_3):n(alcohol)=5:1, WHSV=1.0 h^{-1}	63	[34]
CuZnAlTiLaO_x	315 °C, 0.1 MPa, n(NH_3):n(alcohol)=5:1, WHSV=2.5 h^{-1}	98	[43]
Cu-ZnO-La_2O_3-Al_2O_3	280-290 °C, 0.1 MPa, n(NH_3):n(alcohol)=4-5:1, LHSV=0.25 h^{-1}	96	[44]
CuO-ZnO-ZrO_2/mCaO·nAl_2O_3	280 °C, 0.1 MPa, n(NH_3):n(H_2):n(alcohol)=5:1.15:1, WHSV=1.14 h^{-1}	96	[45]

Table S3. Cu particle sizes of the reduced and spent catalysts [a]

Catalyst	Before reaction (nm)	After reaction (nm)
Cu_{10}/meso SiO_2-IM	46.0	49.4
Cu_{10}-Zr_2/meso SiO_2-IM	43.7	45.5
Cu_{10}-Zr_2/meso SiO_2-UP	--	16.7

[a] Calculated by the Scherrer equation at $2\theta = 43.4^{\circ}$.

Table S4. Textural properties of the catalysts

Catalyst	S_{BET}(m^2/g) [a]	V_{micro}(cm^3/g) [b]	V_{meso}(cm^3/g) [c]	Pore size (nm) [d]
Cu_{10}/meso SiO_2-IM	413.6	0	0.55	4.5
Cu_{10}-Zr_2/meso SiO_2-IM	408.2	0	0.58	4.9
Cu_{10}-Zr_2/meso SiO_2-UP	432.9	0	0.71	5.7
meso SiO_2	475.6	0	0.56	4.6

[a] BET surface area. [b] t-Plot micropore volume. [c] BJH adsorption volume. [d] BJH mesopore size distribution based on the adsorption branch.

Table S5. Chemical composition of the spent catalysts [a]

Catalyst	CuO (%)	ZrO_2 (%)
Cu_{10}/meso SiO_2-IM	6.1	-
Cu_{10}-Zr_2/meso SiO_2-IM	10.2	2.1
Cu_{10}-Zr_2/meso SiO_2-UP	10.3	2.3

[a] Obtained from the ICP analysis.

1. G. C. Chinchen, C. M. Hay, H. D. Vandervell and K. C. Waugh, *J. Catal.* , 1987, **103**, 79-86.
2. J. Gong, H. Yue, Y. Zhao, S. Zhao, L. Zhao, J. Lv, S. Wang and X. Ma, *J. Am. Chem. Soc.* , 2012, **134**, 13922-13925.
3. C. A. Emeis, *J. Catal.* , 1993, **141**, 347-354.
4. K. Trangwachirachai and Y.-C. Lin, *Dalton Trans.* , 2023, **52**, 6211-6225.
5. K. Kim, *J. Catal.* , 1992, **137**, 127-138.
6. K. Trangwachirachai, C.-H. Chen and Y.-C. Lin, *Molecular Catalysis*, 2021, **516**, 111961-111971.
7. D.-C. Kang, E.-J. Kim, D.-P. Kim and C.-H. Shin, *Appl. Catal., A* 2022, **641**, 118688-118698.
8. G. Chen, S. Fadaeerayeni, L. Fang, E. Sarnello, T. Li, H. Toghiani and Y. Xiang, *Catal. Today* 2023, **416**, 113751-113759.
9. F. Ayari, M. Mhamdi, D. P. Debecker, E. M. Gaigneaux, J. Alvarez-Rodriguez, A. Guerrero-Ruiz, G. Delahay and A. Ghorbel, *J. Mol. Catal. A: Chem.* , 2011, **339**, 8-16.
10. B. Rhimi, M. Mhamdi, V. N. Kalevaru and A. Martin, *RSC Adv.*, 2016, **6**, 65866-65878.
11. G. Chen, T. Liang, P. Yoo, S. Fadaeerayeni, E. Sarnello, T. Li, P. Liao and Y. Xiang, *ACS Catal.*, 2021, **11**, 7987-7995.
12. E. Rojas, M. O. Guerrero-Pérez and M. A. Bañares, *Catal. Commun.* , 2009, **10**, 1555-1557.
13. Y. Li and J. N. Armor, *J. Catal.* , 1998, **173**, 511-518.
14. S. Essid, F. Ayari, R. Bulánek, J. Vaculík, M. Mhamdi, G. Delahay and A. Ghorbel, *Solid State Sci.* , 2019, **93**, 13-23.
15. X. Liu, T. Liang, R. Barbosa, G. Chen, H. Toghiani and Y. Xiang, *ACS Omega*, 2020, **5**, 1669-1678.
16. M. O. Guerrero-Pérez, E. Rojas-García, R. López-Medina and M. A. Bañares, *Catal. Lett.* , 2016, **146**, 1838-1847.
17. F. Rubio‐Marcos, E. Rojas, R. López‐Medina, M. O. Guerrero‐Pérez, M. A. Bañares and J. F. Fernandez, *ChemCatChem*, 2011, **3**, 1637-1645.
18. R. Catani and G. Centi, *J. Chem. Soc., Chem. Commun.* , 1991, **16**, 1081-1083.
19. Y. Liu, T. Li, S. Qiao, Z. Heng, T. Zhao, H. Wu, T. Xiong, J. Li, X. Yao, L. Long, Y. Xiang, Q. Liu, L. Lu, T. Liang, J. Chen and F. Jin, *ACS Appl. Mater. Interfaces*, 2023, **15**, 25604-25614.
20. S. I. Galanov, O. I. Sidorova and M. A. Gavrilenko, *Procedia Chemistry*, 2014, **10**, 108-113.
21. E. C. Corker, U. V. Mentzel, J. Mielby, A. Riisager and R. Fehrmann, *Green Chem.* , 2013, **15**, 928-933.
22. D. Wu, J. Li, L. Yao, R. Xie and Z. Peng, *ACS Appl. Mater. Interfaces*, 2021, **13**, 55292-55298.
23. W. Ao, H. Ren, C. Cheng, Z. Fan, Q. Qin, P. Yin, Q. Zhang and L. Dai, *Angew. Chem. Int. Ed.* , 2023, **62**, e202307924.
24. J. Li, J. Tang, D. Wu, L. Yao and Z. Peng, *Int. J. Hydrogen Energy* 2023, **48**, 36286-36294.
25. Y. Zhu, D. Wu, J. Tang, D. Braaten, B. Liu and Z. Peng, *Chem. Commun.* , 2024, **60**, 9007-9021.

26. B. M. Reddy and B. Manohar, *J. Chem. Soc., Chem. Commun.* , 1993, **3**, 234-235.
27. S. J. Kulkarni, R. R. Rao, M. Subrahmanyam and A. V. R. Rao, *J. Chem. Soc., Chem. Commun.* , 1994, **3**, 273.
28. C. Hamill, H. Driss, A. Goguet, R. Burch, L. Petrov, M. Daous and D. Rooney, *Appl. Catal., A* 2015, **506**, 261-267.
29. R. R. Rao, N. Srinivas, S. J. Kulkarni, M. Subrahmanyam and K. V. Raghavan, *Indian. J. Chem. A*, 1997, **36**, 708-711.
30. F. Folco, J. V. Ochoa, F. Cavani, L. Ott and M. Janssen, *Catal. Sci. Technol.*, 2017, **7**, 200-212.
31. T. Tabanelli, M. Mari, F. Folco, F. Tanganelli, F. Puzzo, L. Setti and F. Cavani, *Appl. Catal., A* 2021, **619**, 118139-118150.
32. R. J. Card and J. L. Schmitt, *J. Org. Chem.* , 1981, **46**, 754-757.
33. Y. Hu, J. Cao, J. Deng, B. Cui, M. Tan, J. Li and H. Zhang, *React. Kinet. Mech. Cat.*, 2012, **106**, 127-139.
34. J. Deng, H. S. Zhang, Y. F. Hu, Y. Liu and D. D. Wang, *Adv.Mater. Res.*, 2013, **750-752**, 1700-1703.
35. Y.-S. Jeong, S. H. An and C.-H. Shin, *Korean J. Chem. Eng.* , 2019, **36**, 1051-1056.
36. *Europe Pat.,* EP0206632, 1986.
37. H. Abe and A. T. Bell, *J. Catal.* , 1993, **142**, 430-436.
38. Y. Zhang, Y. Zhang, C. Feng, C. Qiu, Y. Wen and J. Zhao, *Catal. Commun.* , 2009, **10**, 1454-1458.
39. C. Feng, Y. Zhang, Y. Zhang, Y. Wen and J. Zhao, *Catal. Lett.* , 2010, **141**, 168-177.
40. D. Zhang, Y. Zhang, Y. Wen, K. Hou and J. Zhao, *Chem. Eng. Res. Des.* , 2011, **89**, 2147-2152.
41. L. Mei, C. Feng, Y. Wang, Q. Yu, W. Xin, W. Chu, Y. Wang, X. Zhu, S. Liu, H. Wang and L. Xu, *Ind. Eng. Chem. Res.* , 2023, **62**, 14234-14243.
42. X. Li, C. Feng, W. F. Chu, Y. P. Xie, S. L. Liu and X. X. Zhu, *Low-Carbon Chemistry and Chemical Engineering*, 2024, **49**, 28-35.
43. *China Pat.,* CN1062303, 1992.
44. Z. G. Jiang, Y. H. Shan, Y. S. Zhou, Y. Y. Zhang and M. S. Li, *Journal of Changzhou University (Natural Science Edition)*, 2010, **22**, 19-23.
45. V. V. Belov, V. I. Markov, S. B. Sova, E. Z. Golosman and A. I. Nechugovskii, *Russ. J. Appl. Chem.* , 2016, **89**, 414-420.